RF-Egg: An RF Solution for Fine-Grained Multi-Target and Multi-Task Egg Incubation Sensing

Zehua Sun, Tao Ni, Yongliang Chen, Di Duan, Kai Liu, Weitao Xu*
{zehua.sun,taoni2-c,cs.ylchen,dduan5-c}@my.cityu.edu.hk,{kailiu,weitaoxu}@cityu.edu.hk
City University of Hong Kong, Hong Kong, China

ABSTRACT

Eggs and chickens serve as crucial animal-source proteins in our diets, making large-scale breeding egg incubation an essential undertaking. However, current solutions, i.e., vision-based and sensor-based methods, are primarily designed for egg fertility detection tasks under single-egg settings, which have not yet satisfied the goal of multi-target and multi-task sensing. In this paper, we propose *RF-Egg*, the first RF-based fine-grained multi-target and multi-task egg incubation sensing system with respect to sensing fertility, incubation status, and early mortality of chicken embryos. *RF-Egg* leverages the weak coupling effects of RFID tags when interacting with eggs, which induces different impedance changes of RFID tags with the incubation levels of eggs, thereby resulting in a variation of low-level phase readings of the backscatter signals. Regarding the challenge of multi-target profiling interference, we propose a multipath combating algorithm to extract the target-induced signal component based on the built signal model, and address non-uniformity issues across multiple tags. Moreover, we devise three unique feature maps tailored to each task, and then design an Multi-Task Triplet (MTT) network for multitasking. Our evaluation results based on 189 eggs show that *RF-Egg* achieves an accuracy of 94.4%, 96.1%, and 90.1% for the aforementioned three tasks when supporting 16 targets. Additionally, our extensive field study in a local egg hatchery suggests that *RF-Egg* presents the potential to be widely deployed in the modern poultry industry.

*Weitao Xu is the corresponding author.

ACM MobiCom '24, November 18–22, 2024, Washington D.C., DC, USA

ACM ISBN 979-8-4007-0489-5/24/09…$15.00
https://doi.org/10.1145/3636534.3649378

CCS CONCEPTS

• **Computer systems organization** → **Sensors and actuators**; • **Computing methodologies** → **Machine learning**.

KEYWORDS

RFID sensing, Egg incubation

ACM Reference Format:
Zehua Sun, Tao Ni, Yongliang Chen, Di Duan, Kai Liu, Weitao Xu. 2024. *RF-Egg*: An RF Solution for Fine-Grained Multi-Target and Multi-Task Egg Incubation Sensing. In *International Conference On Mobile Computing And Networking (ACM MobiCom '24), September 30–October 4, 2024, Washington D.C., DC, USA.* ACM, New York, NY, USA, 15 pages. https://doi.org/10.1145/3636534.3649378

1 INTRODUCTION

Eggs and chickens are amongst the most important animal-source proteins in our diets. Thus, large-scale breeding egg incubation becomes an essential task to meet the demands of the sustainability of modern poultry production and ensure adequate supply to the consuming population. According to USA Poultry Production and Value 2022 Summary [34], the market value of broilers, turkeys, and eggs has exceeded 77.0 billion dollars in 2022. In the modern poultry industry, large-scale breeding egg incubation requires precisely controlling temperature and humidity levels during a 21-day incubation cycle. Despite the incubation environmental conditions being closely monitored and controlled for incubators [43], there is a lack of sensing systems for assessing the embryo's *multiple* developmental conditions of *multiple* breeding eggs during the entire incubation cycle, with respect to fertility, incubation status, and early mortality.

As shown in Table 1, previous works [14, 15, 25, 37] have made efforts in egg incubation sensing, involving vision-based and sensor-based methods. Specifically, traditional vision-based methods utilize embryo candling [14, 39], hyperspectral imaging [28], and thermal imaging [25] to acquire high-resolution image data for fertility detection. Among these, embryo candling is the most common choice, where an egg is candled by shining a light through it in darkness after day 7 to observe the condition of the air cell, yolk, and white. Conversely, sensor-based methods focus on the variations of inherent properties of eggs during incubation with respect

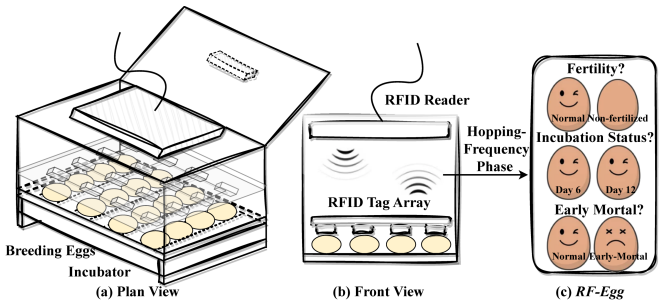

Fig. 1: Illustration of *RF-Egg*. In an incubator with multiple breeding eggs laid flat, an RFID tag array is attached above (rather than sticking to) the eggs. Each tag, corresponding to each egg, responds to the interrogation signal from the RFID reader placed above. According to the readings of the RFID reader, egg incubation sensing tasks can be achieved for multiple eggs with respect to fertility, incubation status, and early mortality.

to oxygen flux [37], acoustic resonance [6], dielectric property [15], and spectral data [10] for fertility detection. For example, the gas exchange rate of an egg is measured in the closed and shielded environment to detect its fertility in [37]. However, existing works are primarily designed for single fertility detection tasks under single-target settings, which have not yet satisfied the goal of multi-target and multi-task sensing. Moreover, the existing solutions fail to meet the necessary requirements regarding non-intrusiveness, responsiveness, and usability.

To take the first step to fill this research gap, we propose *RF-Egg*, an Radio Frequency (RF) solution for fine-grained multi-target and multi-task egg incubation sensing. Specifically, *RF-Egg* exploits the weak coupling effects [16], which results in different impedance changes when interacting with the targets (i.e., eggs), rendering impedance-related phase variations of Radio Frequency Identification (RFID) backscatter signals that could reflect the egg incubation condition. As shown in Fig. 1, in an incubator with multiple breeding eggs laid flat, an RFID tag array is attached above (rather than sticking to) the incubating eggs. Each tag, which corresponds to each egg, responds to the interrogation signal from the RFID reader placed at the top of the incubator. Subsequently, *RF-Egg* leverages the low-level phase features from the captured RFID backscatter signals to achieve multiple egg incubation sensing tasks, in terms of detecting egg fertility, incubation status, and early mortality.

To design *RF-Egg*, we have overcome the following two challenges:

Challenge 1: Multi-target profiling interference. To enable multi-target sensing capability, we propose extending the single-tag sensing approach to the multi-tag one in the spatial dimension. However, for each tag in the tag array, filtering the target-induced signal component from irrelevant ones in multipath environments poses a significant challenge. Thus, we first build a signal model to explicitly understand the various signal components. Following that, we propose a circle-fitting algorithm to filter out the irrelevant components by leveraging on a particular observation: the received signals from the specific tag share the same Received Signal Strength (RSS) values (i.e., signal amplitude), but exhibit phase variations within a 21-day incubation cycle. Moreover, the initial phase and the amount of phase variation across each tag introduce non-uniformity. Thus, we design a series of approaches, such as phase calibration and masking, to standardize the phase information across all tags.

Challenge 2: Multi-task sensing designing. Egg incubation sensing presents us with three distinct tasks with respect to detecting egg fertility, incubation status, and early mortality. Designing a model capable of effectively handling these three tasks presents a challenge. To achieve this, we first devise three unique feature maps: Differencing Map (DM), Global Map (GM), and Cumulative Difference Map (CDM), tailored to each task by exploring the signal variations of three types of eggs. Subsequently, we propose an Multi-Task Triplet (MTT) network, where the multitasking module is designed to leverage the inherent relationships among three task feature maps, while the triplet-picking module addresses the issue of high sample similarity between two classes. MTT is optimized through the use of weighted triplet loss and cross-entropy loss function to indicate task weight, allowing it to avoid task imbalance problems.

We implement *RF-Egg* using commodity RFID hardware and evaluate its performance by conducting comprehensive benchmark experiments with 189 eggs under various impacting scenarios. The results show that *RF-Egg* can achieve an accuracy of 94.4%, 96.1%, and 90.1% for the three tasks when supporting an incubator that can host 16 targets simultaneously. Additionally, our field study in a local egg hatchery attains an average performance of 86.4% for the three tasks.

In summary, *RF-Egg* makes the following contributions:

- To the best of our knowledge, *RF-Egg* represents the first RF-based fine-grained multi-target and multi-task egg incubation sensing system, possessing the characteristics of non-intrusiveness, high-responsiveness, and well-usability. We first demonstrate the feasibility of exploiting low-level phase readings of the RFID backscatter signal in egg incubation sensing, and then advance the sensing capability of *RF-Egg* to the level of multi-target and multi-task sensing.
- Regarding multi-target profiling interference, we propose a novel multipath combating algorithm to extract the target-induced signal component based on the built signal model and design a series of approaches to address non-uniformity

Table 1: Comparison with related egg incubation sensing works in five metrics. M1: multi-target, M2: multi-task, M3: non-intrusiveness, M4: responsiveness, M5: usability (●–True, ❍–False).

Related Works	Type	Feature	M1	M2	M3	M4	M5
Liu et al. [28]	Vision	Hyper-spectral image	●	❍	●	●	❍
Lin et al. [25]	Vision	Thermal image	●	❍	●	●	❍
DPSA [14]	Vision	Embryo image	❍	❍	●	●	●
Saifullah et al. [39]	Vision	Embryo image	❍	❍	●	●	●
Coucke et al. [6]	Sensor	Acoustic resonance	❍	❍	❍	●	❍
NMT-ETS [37]	Sensor	Oxygen flux	❍	❍	●	❍	❍
Ghaderi et al. [15]	Sensor	Dielectric property	❍	❍	❍	❍	❍
Dong et al. [10]	Sensor	Spectral data	❍	❍	●	❍	❍
***RF-Egg* (ours)**	RF	RFID phase	●	●	●	●	●

issues across multiple tags. Regarding three distinct tasks in egg incubation sensing, we design an MTT network to consider task-specific input and task imbalance problems.
- We implement and evaluate *RF-Egg* using commodity RFID hardware. The results show that *RF-Egg* can achieve an accuracy of 94.4%, 96.1%, and 90.1% for the three tasks when sensing 16 targets. Furthermore, our field study suggests that *RF-Egg* presents the potential to be widely deployed in the modern poultry industry.

The rest of this paper is organized as follows: §2 introduces preliminaries. §3 provides sensing models. §4 illustrates system designs of *RF-Egg*, encompassing two components in §5 and §6. §7 presents evaluation results. §8 discusses limitations and future works. §9 summarizes the related works. §10 concludes this paper.

2 PRELIMINARIES

In this section, we give a brief preliminary of egg incubation and RFID system.

2.1 Egg Incubation

Egg structure. Eggs, produced by a chicken, are the contents of hard-shelled reproductive bodies, serving a primary role in both species reproduction and food sources. Typically, an egg weighs 40 g to 60 g, comprising various components including up to 11% lipids, 12% protein, and 74% water [17]. As illustrated in Fig. 2, the primary structural components of an egg include the shell to provide protection for the egg, the albumen to supply water, the yolk to deliver essential nutrients for embryo development, the chalaza to anchor the yolk to the egg's center, and the germinal disc as the embryo-forming part on the egg yolk.

Egg incubation process. Before incubation, breeding eggs are meticulously collected and stored in a cool and dry environment for seven days to promote natural development and maturation. During the first 18 days of incubation, the eggs are placed lying horizontally, turned intermittently within the incubator set in a constant temperature 37.8 °C and relative humidity of 60%. During the last three days, egg turning ceases, and the eggs are positioned with their larger ends facing upward while maintaining temperature and increasing relative humidity, awaiting the chicks to hatch.

As illustrated in Fig. 3, the egg incubation process typically spans 21 days [42]. During the initial three days of incubation, the embryo's tissues, blood vessels, and heart begin to develop, giving rise to the initial characteristics of the embryo. On days 4–9, the embryo has eye pigmented, and grows various organs with respect to elbows, knees, beak, and feather bundles sequentially, rendering bird-like appearances. On days 10–12, the organs continue to grow, resulting in protruding teeth, evident tail feathers, and the formation of toes. On days 13–18, the embryo moves towards the larger end of the egg, feathers emerge then fully cover the entire body, and egg albumen almost vanishes, indicating complete development. During the last three days of incubation, the yolk sac is completely drawn in, and the embryo occupies the entire egg, which is now ready to break out of its shell. Throughout this process, the egg undergoes a significant qualitative biological change. Intriguingly, these internal changes have a significant impact on the egg's dielectric permittivity [2, 4], a factor crucial to *RF-Egg* (§2.2).

2.2 RFID

RFID system. A typical RFID system, as illustrated in Fig. 4, comprises readers with antennas (or interrogators) and passive electronic tags (or transponders). The communication and energy supply between the reader and the tag are accomplished by electromagnetic backscatter coupling [8]. Specifically, the passive tag captures the query RF signal emitted by the reader whilst harvesting energy to power itself, and then modulates the response backscatter signal by changing its antennas' impedance.

Weak coupling effect between the tag and the target. When the RFID tag is positioned in close proximity to the target, even without direct contact, the tag antenna's interaction with the target in its immediate vicinity is governed by a concept called a near-field inductive coupling effect [16]. The reason is that the electromagnetic field of the RFID tag antenna is occupied by the region of space at which the target is located. Specifically, the extent of the coupling effect is largely determined by an intrinsic property of the target known as dielectric permittivity [2, 4], represented as ϵ_r. The dielectric permittivity describes the medium's capacity to store electric field energy relative to a vacuum. As the dielectric permittivity of incubating eggs will change with their incubation level, thus affecting the electric field distribution around the egg.

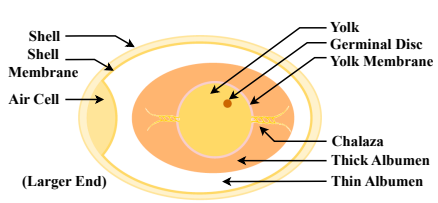

Fig. 2: The structure of an egg.

Fig. 3: Egg incubation process.

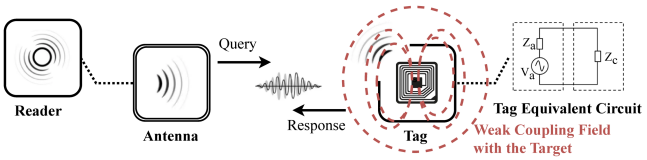

Fig. 4: RFID system.

This variation induces a change in the impedance-related phase, which can be leveraged for egg incubation sensing.

2.3 Feasibility Study

Enabling RFID sensing capability in egg incubation is desirable, prompting us to conduct a feasibility study to verify our concept. In our experiment, we attach a passive RFID tag near (rather than sticking to) the breeding eggs to interact with the reader, which records the low-level channel features of the RF signal during a 21-day incubation cycle. Three types of eggs are accounted for: non-fertilized, early-mortal, and normal breeding eggs, and examine their signal variations within a 21-day period. Using collected signals, we explore the possibility of (1) detecting egg fertility, (2) monitoring egg incubation status, and (3) identifying embryo early mortality. Fig. 5 demonstrates the RF signal phase readings during a 21-day incubation period.

Task 1: Detecting egg fertility. As shown in Fig. 5, the difference in signal phase values between non-fertilized and normal breeding eggs is noticeable. The phase curve of the non-fertilized eggs shows stable values over time, while that of the normal breeding ones shows a trend of variation as the incubation level changes, rendering a not overlapping of incubation and non-fertilized zones. As a result, this difference indicates that non-fertilized and normal breeding eggs produce distinct features on and after day 4.

Task 2: Monitoring egg incubation status. Our focus then moves to the signal phase variation of normal breeding eggs during a 21-day period. It is observed the different incubation levels result in different variations in signal phase readings. Intuitively, phase values have an increasing trend during the entire period, which can be leveraged to accurately monitor the specific egg incubation status. The increasing phase trend is mainly attributed to the reduction of egg's permittivity, i.e., the alterations in less water (high permittivity) and more embryos (low one).

Task 3: Identifying embryo early mortality. Lastly, we focus on the difference between early-mortal and normal breeding eggs. We can observe that the phase curves of both types of eggs diverge from a certain point (i.e., day 10) and subsequently show different patterns over time. This point represents the date of death of the egg embryo, while the early-mortal zone presents its different development compared with a normal breeding egg. This difference indicates that embryo early mortality can be identified.

Key insights. Our key insights are summarized as follows. The qualitative changes occurring inside eggs at various incubation levels cause unique RF signal phase variation. This validates the feasibility of exploiting fine-grained phase features of the RF signal to detect egg fertility, monitor egg incubation status, and identify embryo early mortality. The underlying rationale is weak coupling effects result in different impedance-related phase variations of RFID backscatter signals when interacting with eggs. As such with these insights, our goal is to advance the sensing capability from single-target to multi-target, and from single-task to multi-task.

3 UNDERSTANDING MULTI-TARGET SENSING

To enable multi-target sensing capability, we propose extending the single-tag sensing approach to the multi-tag one in the spatial dimension. By assigning each tag to a distinct target to capture their respective RF signal variations, we can achieve multi-egg incubation sensing. Specifically, we lay out a tag array Γ with the size of $h \times w$ ($h, w > 0$). Each tag element in Γ can be denoted as $\gamma(i, j)$, where $i = 1, 2, \ldots h$; $j = 1, 2, \ldots w$, representing its location in the tag array and the corresponding situated breeding egg.

Transmission model. In an RFID system built with passive tags, when the reader interrogates the tags, the query signal transmitted by the reader can be represented as $S_{Tx} = |S_{Tx}|\, e^{j\theta_{Tx}}$, where $|S_{Tx}|$ and θ_{Tx} represent the signal's amplitude and phase, respectively. Then, the received signal at the tag $\gamma(i, j)$ side can be represented as

$$S_{Tag}(i, j) = S_{Tx} \cdot h_{Air}(i, j) \cdot h_{Tag}, \tag{1}$$

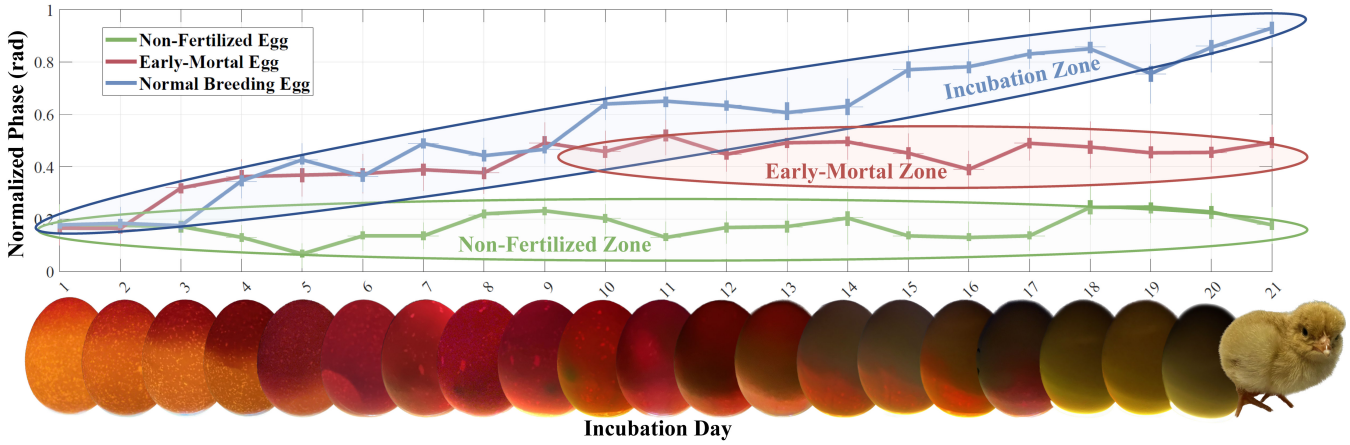

Fig. 5: Illustration of RF signal phase variations of non-fertilized, early-mortal (from day 10), and normal breeding eggs during a 21-day incubation period (top), along with the candling figures of normal breeding eggs (bottom).

where $h_{Air} = |h_{Air}| \cdot e^{j\theta_{Air}}$ and $h_{Tag} = |h_{Tag}| \cdot e^{j\theta_{Tag}}$ represent the channel parameters over the air and the tag's antenna [46], respectively.

When the RFID tag receives the query signal, it modulates the reflection backscatter signal controlled by its tag chip. The reflection coefficient $F = |F| \cdot e^{j\theta_F}$, is a measure of the impedance mismatch between the tag's antenna and the RFID chip [36]. Thus, the received signal at the reader side from the tag $\gamma(i,j)$ can be represented as

$$\begin{aligned} S_{Rx}(i,j) &= S_{Tag}(i,j) \cdot F(i,j) \cdot h_{Air}(i,j) \cdot h_{Rdr} \\ &= \left|F(i,j) S_{Tx} h_{Air}(i,j)^2 h_{Tag} h_{Rdr}\right| e^{j\left(\theta_F(i,j)+\theta_{Tx}+2\theta_{Air}(i,j)+\theta_{Tag}+\theta_{Rdr}\right)}, \end{aligned} \tag{2}$$

where $h_{Rdr} = |h_{Rdr}| \cdot e^{j\theta_{Rdr}}$ represents the channel parameters over reader's antenna.

Throughout our experiments, we have maintained the experiment settings while the incubation level of the eggs varied. Thus, S_{Tx}[1], h_{Tag}[2], and h_{Rdr} are regarded as constants. The factors subject to variation are $F(i,j)$ due to the tag impedance change, and $h_{Air}(i,j)$ due to the multipath signal propagation change.

Tag impedance. As stated in §2.2, the presence of the target alters the tag's antenna impedance due to the weak coupling effect, and subsequently the reflection coefficient F. Specifically, as illustrated in Fig. 4, a passive RFID tag comprises an antenna and an Integrated Circuit (IC), with their impedance denoted as Z_c and Z_a, respectively. Notably, the IC chip has two impedance states, i.e., $Z_c(On)$ and $Z_c(Off)$. Thus, F can be then represented as [33, 36]:

$$|F| = \left|\frac{Z_c - Z_a^*}{Z_c + Z_a}\right|, \theta_F = \arg\left(\frac{1}{Z_a + Z_c(Off)} - \frac{1}{Z_a + Z_c(On)}\right). \tag{3}$$

It follows then, that the reflection coefficient $F(i,j)$ is influenced by the incubation level of the corresponding breeding egg situated at tag $\gamma(i,j)$, thereby rendering an RF signal variation.

Multipath signal propagation. The received signal is typically the superposition of signals from multiple Line-Of-Sight (LOS) direct and Non-LOS (NLOS) indirect paths, referred to as multipath. As illustrated in Fig. 7, the received signal can be decomposed into three components: direct LOS component h_{Los}, the target-induced component h_{Tar}, and surrounding environment components h_{Env} such as nearby eggs, incubator shells, and the tag pad. Given the interfering components h_{Los}+h_{Env} may cause unpredictably signal variations, our goal is to focus only on target-induced components h_{Tar}. Thus, the multipath effect can be represented by

$$\begin{aligned} h_{Air} &= h_{Los} + h_{Tar} + h_{Env} \\ &= |h_{Tar}| e^{j\theta_{Tar}} + \sum_{i}^{n} |h_i| e^{j\theta_i}, \end{aligned} \tag{4}$$

where n is the total number of signal propagation paths other than target-induced one, and h_i is the channel coefficient of path i.

The theoretical principle of h_{Tar} is described as follows. When an RF signal encounters a boundary between the air and the solid surface of an egg, a portion of the wave is transmitted into the egg, while another portion of the wave is reflected back into the air (and received by the tag). The reflection coefficient R describes the ratio of the reflected waves to the incident ones, which can be expressed as $R = \frac{Z_2 - Z_1}{Z_2 + Z_1}$,

[1] RFID readers typically transmit signals with a fixed phase to ensure highly accurate signals to be received by tags [8].

[2] h_{Tag} mainly represents the channel parameters of the tag's antenna with respect to gain, polarization, and radiation efficiency.

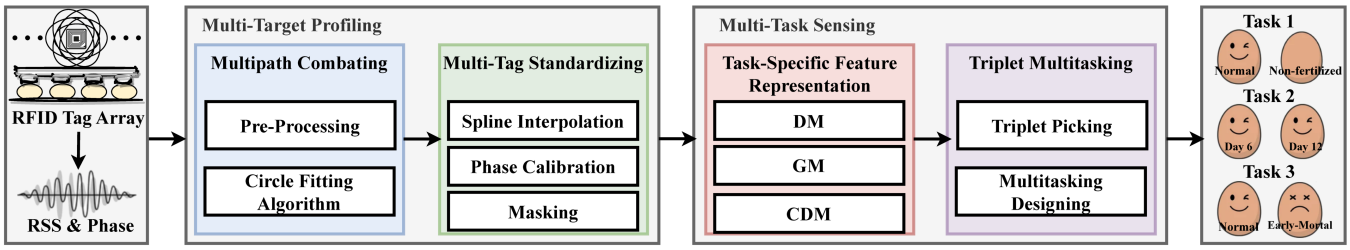

Fig. 6: System overview of *RF-Egg*. Specifically, *RF-Egg* works in two stages: multi-target profiling and multi-task sensing stages.

where Z_1 and Z_2 are the impedance of the air and egg, respectively. The impedance Z is related to the refractive index r through $Z = \sqrt{\mu_0/\epsilon_0} \cdot r$, where μ_0 and ϵ_0 are the permeability and permittivity of free space, respectively. The refractive index r is an intrinsic characteristic of the medium related to its complex permittivity ϵ_r, which can be written as $\epsilon_r = \epsilon_r' + i\epsilon_r''$ [49], where ϵ_r' and ϵ_r'' represent the real and imaginary parts. The refractive index r can then be expressed as

$$r = \sqrt{\frac{1}{2}\left(\sqrt{(\epsilon_r')^2 + (\epsilon_r'')^2} + \epsilon_r'\right)}. \tag{5}$$

As stated previously, the dielectric permittivity ϵ_r of breeding eggs varies with their incubation level, which affects the refractive index r, and subsequently the reflection coefficient R. Consequently, the target-induced component h_{Tar} is slightly influenced by the level of egg incubation, rendering an RF signal variation.

However, irrelevant components $h_{Los} + h_{Env}$ are not modeled to quantify their adverse effects on the measured sensing results. Thus, isolating the target-induced signal component from irrelevant ones poses a primary challenge, the detailed solution is presented in §5.1.

4 *RF-EGG* DESIGN

Fig. 6 illustrates the system overview of *RF-Egg*. *RF-Egg* works in two stages: multi-target profiling and multi-task sensing stages.

Multi-target profiling. Upon receiving the RSS and phase readings captured by the RFID tag array when interacting with the eggs, they are pre-processed to form complex signals. Following this, we propose a circle fitting algorithm to filter out the irrelevant signal components, as detailed in §3. Subsequently, we devise a series of countermeasures, such as spline interpolation, phase calibration, and masking, to standardize the phase information across all tags in the tag array.

Multi-task sensing. In this stage, the signals, after being processed by the multi-target profiling stage, are further leveraged to generate DM, GM, and CDM for each of the three tasks, respectively. Subsequently, these feature maps are fed into the proposed MTT network, where the multitasking module is engineered to leverage the inherent relationships among three task feature maps, while the triplet picking module addresses the issue of high sample similarity between two classes. Finally, *RF-Egg* can achieve fertility, incubation status, and early mortality sensing for multiple breeding eggs.

5 MULTI-TARGET PROFILING

In this section, we discuss the process of multi-target profiling, including multipath combating (§5.1) and multi-tag standardizing (§5.2).

5.1 Multipath Combating

5.1.1 Pre-Processing. We start by pre-processing the received RSS and phase readings for the proposed multipath combating methods. As stated previously in §3, we possess a tag array Γ containing multiple tags $\gamma(i, j)$, sized $h \times w$. The tag array captures a data segment $\mathcal{D} = \{\mathcal{R}, \mathcal{P}\}$ over c hopping frequencies (the channel index is represented by k), where RSS and phase data stream are denoted as $\mathcal{R} = \{\mathcal{R}(i, j, k)\}$ and $\mathcal{P} = \{\mathcal{P}(i, j, k)\}$, respectively. Subsequently, we leverage the data segment $\mathcal{D}$ to construct the received complex signals $S_{Rx}(i, j, k)$ for the tag $\gamma(i, j)$ over the $k-th$ hopping frequency. However, the received signals are prone to distortion caused by environment noises. Moreover, the movement of embryos in the breeding eggs can also cause signal fluctuations. As such, we use the Savitzky-Golay (S-G) filter [30] to diminish ambient noise and limit signal fluctuations, while not introducing additional phase distortion problems.

5.1.2 Circle Fitting Algorithm. To better explain the multipath effect in RFID system, we utilize the example shown in Fig. 8 to illustrate the phase variation of RF signals over 16 hopping frequencies (from 920.625 MHz to 924.375 MHz) when direct-path and multipath signals dominate, respectively. It is observed that the direct-path signal results in an approximate linearly-changing phase across the frequency

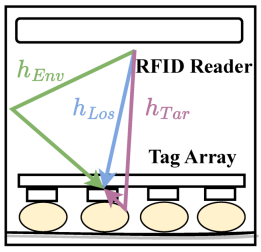

Fig. 7: Multipath signal propagation.

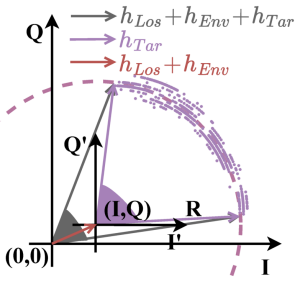

Fig. 9: Circle-fitting algorithm.

bands, while severe multipath signals may cause unpredictable signal variation to adversely affect phase measurements. Consequently, eliminating the influence induced by irrelevant multipath signals has a significant impact on the sensing accuracy.

To achieve this, an intuitive method [50] is leveraging the linear phase-frequency relationship to select specific channels with little multipath. However, this approach still includes irrelevant components and cannot specify the same channel indices when sensing multiple targets. To this end, we propose a novel multipath combating algorithm as a reliable solution.

Key observations. Revisiting in §3, the received complex signal comprises both the target-induced component h_{Tar} and irrelevant components $h_{Los}+h_{Env}$. Thus, the received signal is the superposition of these two components, which can be depicted in the Inphase-Quadrature (I-Q) plane, as illustrated in Fig. 9. To filter out the irrelevant components$h_{Los}+h_{Env}$, we adopt the circle fitting algorithm [12] to separate these two components. Our algorithm is based on two key observations. (1) As we kept the experiment settings invariant with no significant displacement among the reader, tags, and targets, thus the irrelevant components $h_{Los}(i,j)+h_{Env}(i,j)$ for each tag $\gamma(i,j)$ in Γ can be roughly considered constant. While the incubation level of the breeding eggs within a 21-day incubation cycle varies, the target-induced component $h_{Tar}(i,j)$ resulted from the corresponding breeding egg varies. (2) The received signals from the same breeding egg share the same RSS values (i.e., signal amplitude)[3], but exhibit phase variations within a 21-day incubation cycle. Therefore, the received signals $S_{Rx}(i,j,k)$ are distributed over part of the arc on a circle, since they have the same circle center (due to constant irrelevant components $h_{Los}+h_{Env}$), the same radius but varying phase values (due to invariant amplitudes but variant phases of the target-induced component h_{Tar}). Thus, we identify the center of the circle corresponding to

[3]According to signal model in §3, although signal amplitude may vary, its variation is far from significant compared to the fine-grained phase.

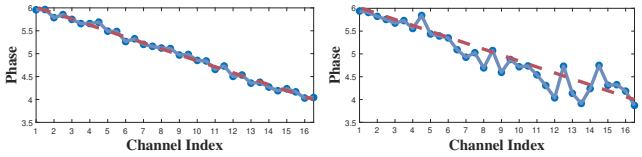

(a) Direct-path signals dominate. (b) Multipath signals dominate.

Fig. 8: RFID signal phase variation over 16 hopping frequencies.

irrelevant components $h_{Los}(i,j)+h_{Env}(i,j)$, which is then utilized as the new coordinate origin to extract the target-induced component $h_{Tar}(i,j)$ for each tag $\gamma(i,j)$ in Γ.

Circle fitting algorithm. Fig. 9 illustrates the process of the least squares circle fitting algorithm. For the tag $\gamma(i,j)$, we collect the signals $S_{Rx}(i,j,k)$ over a 21-day incubation cycle. This allows us to generate a set of points $[X,Y]$ in the I-Q plane, where $X=[x_1,x_2,\ldots,x_n]^{\mathrm{T}}$ and $Y=[y_1,y_2,\ldots,y_n]^{\mathrm{T}}$ represent the real and imaginary parts of a total of n sampling points from the signals. Thus, the equation of the fitting circle can be represented by

$$X^2+Y^2-2IX-2QY+(I^2+Q^2-R^2)=0, \tag{6}$$

where I and Q represents the coordinates of circle's center while R is its radius. The equation can be rewritten as:

$$\begin{bmatrix} x_1^2+y_1^2 \\ x_2^2+y_2^2 \\ \vdots \\ x_n^2+y_n^2 \end{bmatrix} + \begin{bmatrix} x_1 & y_1 & 1 \\ x_2 & y_2 & 1 \\ \vdots & \vdots & \vdots \\ x_n & y_n & 1 \end{bmatrix} \times \begin{bmatrix} -2I \\ -2Q \\ I^2+Q^2-R^2 \end{bmatrix} = 0. \tag{7}$$

By solving these equations via Newton's method [3], we can obtain the fitted circle. Specifically, we subtract the circle center $[I,Q]$ from the original points $[X,Y]$ to obtain the new points, i.e., $[X',Y']=[X,Y]-[I,Q]$, which represents the target-induced components of the received signals, denoted as $S'_{Rx}(i,j,k)$.

5.2 Multi-Tag Standardizing

Given our use of a multi-tag array for sensing, we encounter three problems in non-uniformity across tags: the response sequences, the initial phase after multipath combating, and the amount of phase variation.

Spline interpolation. The response sequences of RFID tags exhibit non-uniformity in the time domain [52], due to different signal paths and intra-signal interference. To address this issue, we perform spline interpolation [49] to re-sample the signal $S'_{Rx}(i,j,k)$. This involves approximating the values between the original data points by a series of spline functions to obtain continuous smooth signals. By doing so, we obtain the re-sampled one possessing the same length L for each tag.

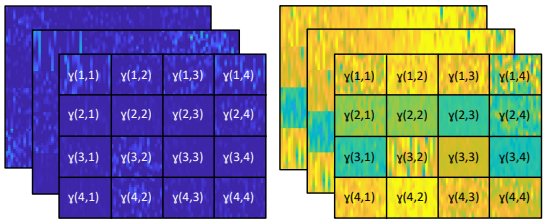

(a) Day 1. (b) Day 21.

Fig. 10: Illustration of GM of the tag array Γ with the size of $h \times w$ over c hopping frequencies on day 1 and day 21, respectively ($h = w = 4$ and $c = 3$).

Phase calibration. After combating the multipath effect, the sampling points of the re-sampled signal $S'_{Rx}(i, j, k)$ of the tag $\gamma(i, j)$ are distributed within approximately the same range on the circle in the I-Q plane. However, those of different tags are distributed within different ranges on the circle due to different signal paths, rendering different phase offsets. To rectify this, we perform phase calibration by rotating the phases of the signals of different tags from the same starting position (i.e., from around 0) to enable accurate and reliable multi-target sensing.

Masking. In our tag array Γ, the amount of phase variation caused by the breeding eggs situated at different tag locations is not uniformly the same over a 21-day incubation cycle (see Fig. 10). Therefore, we aim to incorporate location information to counteract this effect. Specifically, we first reshape the 1D phase sequence of the calibrated signal $S'_{Rx}(i, j, k)$ into a 2D matrix, consequently producing the block $\mathcal{B}(i, j, k)$ of size $\sqrt{L} \times \sqrt{L} \times k$. Thus, we can collect phase blocks $\mathcal{B}$ (i.e., GM in §6.1) of the tag array Γ with the size of $h \times w$ over c hopping frequencies, as shown in Fig. 10.

Therefore, we employ the mask mechanism [53] to emphasize the phase blocks $\mathcal{B}(i, j)$ of the targeted tag location $\gamma(i, j)$ while those of other blocks are set to a weight of 0. This mask mechanism allows preserving the tag location information whilst serving the task-specific feature representation.

6 MULTI-TASK SENSING

In this section, we discuss the process of multi-task sensing, including task-specific feature representation (§6.1), and triplet multitasking (§6.2).

6.1 Task-Specific Feature Representation

DM for Task 1. Revisiting *S*2.3, the signal phase of non-fertilized and normal breeding eggs shows a noticeable difference. The approach hence involves creating a DM, achieved by subtracting the phase block $\mathcal{B}(i, j)$ of a reference non-fertilized egg from that of the candidate egg.

GM for Task 2. As determined by our feasibility study, the phase values of normal breeding eggs exhibit an increasing trend with the incubation level. However, this variation is fine-grained and susceptible to various noise or improper measurement operations. In practice, the incubation status of the eggs in the same batch is typically consistent. To improve the robustness of *RF-Egg*, we devise a GM that takes into account all blocks $\mathcal{B}$ as shown in Fig. 10. Even if non-fertilized and early-mortal eggs may be present, their proportion is relatively small.

CDM for Task 3. Identifying embryo's early mortality poses a significant challenge, as often a single signal collection fails to provide sufficient information. For example, as depicted in Fig. 5, ideally, one single signal collection would regard the day of early mortality as its current incubation status, rather than acquiring its embryo development condition. Therefore, we design a d Cumulative Difference Map (d-CDM) that aggregates the DM of the candidate egg with those from its previous d days to identify embryo early mortality.

6.2 Triplet Multitasking

Once generating the task-specific feature maps, we need to design a network tailored to our incubation sensing tasks. However, this presents two significant challenges:

(1) When considering three distinct tasks, a straightforward approach is to treat them as separate tasks to be solved independently, which disregards the valuable correlation information existing between the tasks [44]. In this respect, multi-task learning [24] emerges as a potential solution, which aims to enhance task performance and model generalization by jointly training multiple related tasks to thereby exploit their intrinsic relationships and specific information [44]. In our approach, we design a multi-task neural network with hard constraints [57], which allows all tasks to learn task-shared features by sharing some identical bottom layers while each task to learn task-specific features by applying unique layers to each sub-network for a specific task.

(2) When performing Task 2, it is common to encounter highly similar samples between two classes, such as samples from adjacent incubation days, which can blur the boundary between two classes. To address this issue, we utilize a triplet network [40] to alleviate such a problem. A triplet network, a type of neural network used in metric learning, is designed to learn a similarity function that maps inputs into a metric space, where the distance between inputs reflects their similarity. By leveraging a triplet network, we can enhance the accuracy of classification tasks, even those with numerous sample classes and limited data. Overall, we propose an MTT network for our incubation sensing tasks below.

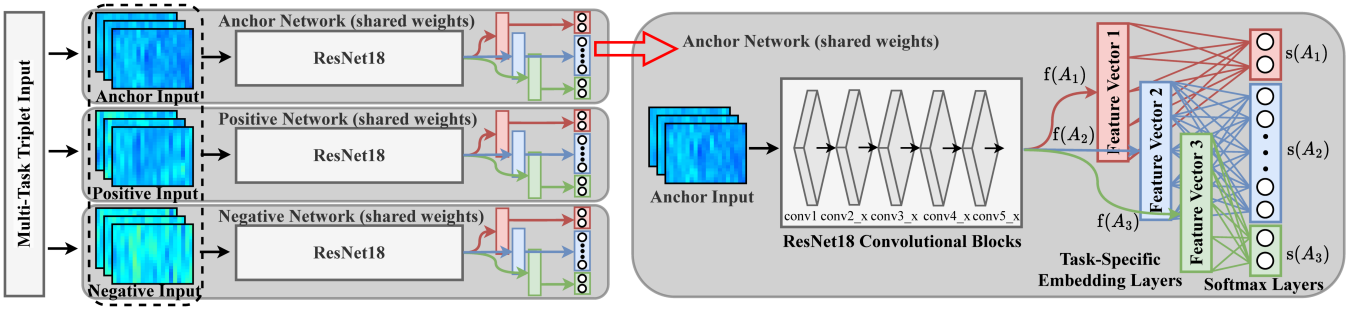

Fig. 11: Multi-Task Triplet (MTT) network.

Network architecture. Fig. 11 illustrates the architecture of the proposed MTT network. The MTT network is composed of three parallel and identical sub-networks that serve as feature extractors, sharing the same weights and hyperparameters. Thus, it processes three distinct inputs, namely the anchor (A), positive (P), and negative (N) inputs, each of which is independently fed into its respective sub-networks. Each sub-network takes the ResNet18 network [19] as the backbone. Specifically, each ResNet18 backbone maintains its pre-existing architecture until the fully connected layers. Specifically, they each possess three parallel fully connected layers as the embedding layers, followed by three parallel softmax layers corresponding to the class number of each task (i.e., 2, 21, and 2). Among these components, the ResNet18 pre-existing architecture, until the fully connected layers, is responsible for learning shared correlation features, the embedding layers are designed to extract task-specific features across tasks, while the softmax layers are for classification.

Triplet picking. Specifically, the triplet inputs are defined as follows:

- **Anchor.** The anchor input serves as the main reference point.
- **Positive.** The positive input is randomly selected from the remaining samples of the anchor's class.
- **Negative.** The negative input is sampled from any other class from the anchor in the same task. We focus on samples from two adjacent incubation days.

Training strategy. The training objective for each task is two-fold: (1) to minimize the distance between the anchor A and the positive P and to maximize the distance between A and the negative N; and (2) to minimize the discrepancy between predicted output and actual label. The triplet loss function $\mathcal{L}_{tri}(A, P, N)$ can be formulated as:

$$\mathcal{L}_{tri}(A,P,N) = \max\left(\|\mathrm{f}(A) - \mathrm{f}(P)\|_2 - \|\mathrm{f}(A) - \mathrm{f}(N)\|_2 + \epsilon, 0\right), \quad (8)$$

where ϵ represents the margin between the positive P and negative N pairs, and f is the embedding feature vector. While, the cross-entropy loss function $\mathcal{L}_{ce}(A_t)$ for task t can be expressed as:

$$\mathcal{L}_{ce}(A_t) = -\sum_{i=1}^{C} A_{ti} \log(\mathrm{s}(A_{ti})), \quad (9)$$

where C is the number of classes, A_{ti} represents whether the sample belongs to class i (i.e., 0 or 1), and $\mathrm{s}(A_{ti})$ is the predicted output from the softmax layer. The loss value for each task is calculated independently, utilizing its own class score. These separate loss values from all tasks are then added together to determine the total loss of the MTT network during the training process, which is instrumental in learning the network parameters. This can be expressed as:

$$\mathcal{L}(A,P,N) = \sum_{t=1}^{3} \lambda_t \left(\mathcal{L}_{tri}(A_t, P_t, N_t) + \mathcal{L}_{ce}(A_t)\right), \quad (10)$$

where t is the index of task, λ_t represents the weight of the corresponding task. For our purposes, Task 2 is identified as the primary task.

7 EVALUATION

In this section, we evaluate the performance of *RF-Egg*, including experimental methodology (§7.1), overall performance (§7.2), micro-benchmarking (§7.3), and field study (§7.4).

7.1 Experimental Methodology

Hardware platform. As shown in Fig. 12 (a), we implement *RF-Egg* using a Commercial Off-The-Shelf (COTS) Impinj Speedway R420 RFID reader equipped with a single directional circularly-polarized antenna (with the gain of 9 dBi and beamwidths of 70° in elevation and azimuth directions), multiple Alien AZ-9629 RFID tags (measuring 22.5 mm × 22.5 mm in size). The RFID reader interfaces with a computer equipped with Intel Core i7-10700 2.90 GHz CPU, 64 GB RAM, and NVIDIA GeForce RTX 3080 GPU, acting as a server via an Ethernet cable.

Backend implementation. The server establishes the connection with the RFID reader under Low-Level Reader Protocol (LLRP) for data collection, where the software facilitating

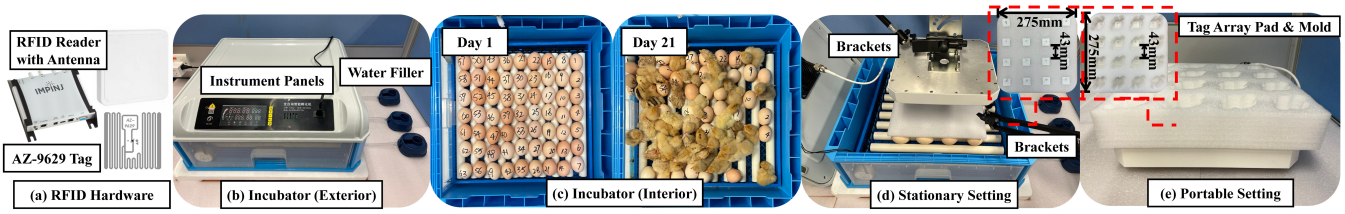

Fig. 12: Experimental setup, including RFID hardware, incubator (exterior and interior), and *RF-Egg* (Stationary and Portable settings).

this communication is developed using C#. Additionally, the multi-target profiling and multi-task sensing algorithms are implemented in Matlab and Python.

Experimental setting. As shown in Fig. 12 (b) and (c), we evaluate *RF-Egg* in the context of an incubator containing multiple breeding eggs[4]. *RF-Egg* is designed with two distinct configurations: a Stationary one (*RF-Egg-S*) and a Portable one (*RF-Egg-P*), which are shown in Fig. 12 (d) and (e), respectively. The Stationary setting is tailored for use within incubator environments, while the Portable setting is more suited to field-study environments. In the Stationary setting, where the eggs are laid flat in the incubator, a tag array pad is attached above the eggs. Each tag, which corresponds to each egg, responds to the interrogation signal from the RFID reader suspended above. Conversely, in the Portable setting, the eggs are positioned horizontally in a tag array mold. Each tag is located underneath the grooves of the eggs and responds to the interrogation signal from the RFID reader situated underneath.

By default, the server continuously receives the RSS and phase readings from multiple tags across 16 hopping frequencies from 920.625 MHz to 924.375 MHz with a channel bandwidth of 250 KHz. The transmission power is set at 30 dBm, with a TX-RX distance of 7 cm for *RF-Egg-S* and 1 cm for *RF-Egg-P*, respectively.

Data collection. To evaluate *RF-Egg*, we conducted three iterations of the egg incubation process, yielding a total of $63 \times 3 = 189$ candidate eggs. These eggs, chosen to be as diverse as possible in terms of weight and shape, are outlined in Table 2. The groundtruth is determined based on the condition of the eggs at the end of the incubation process, along with the candlelight detection procedure. Under both the Stationary and Portable settings, we collect data at 10 AM and 10 PM each day, five samples for each time, over a 21-day incubation cycle, accumulating a total of $189 \times (5+5) \times 21 = 39,690$ samples. For each task, we randomly designate 80% sample data as the training set, while the remaining 20% data forms the test set, with a guarantee that there is no intersection between the two sets.

Performance metrics. The performance metrics are as follows:

- **Accuracy (Acc.):** the ratio of correctly classified samples over the total number of samples, used for the three tasks.
- **False Reject Rate (FRR):** the ratio that a normal breeding egg is classified as a non-fertilized/early-mortal one, used for Task 1 and Task 3.
- **Mean Absolute Deviation (MAD):** the daily-based mean deviation between classified results and the true labels, used specially for Task 2.

7.2 Overall Performance

Fig. 13, 14 and 15 illustrate the overall performance of *RF-Egg* with respect to three tasks, across varying numbers of multi-targets (i.e., 1, 4, 9, 16) under two distinct settings.

Result of Task 1. For Task 1, *RF-Egg* has achieved promising results across varying numbers of multi-targets, i.e., an average Acc. of 95.8% and 96.7%, and an average FRR of 1.7% and 1.3%, for *RF-Egg-S* and *RF-Egg-P*, respectively. With one single sensing target, the Acc. of *RF-Egg-S* and *RF-Egg-P* is 97.7% and 98.3%, respectively. However, it drops to 93.1% for *RF-Egg-S* and 94.4% for *RF-Egg-P* when sensing 16 targets simultaneously. In parallel, the FRR for *RF-Egg-S* and *RF-Egg-P* with a single target is 0.8% and 0.5%, respectively, but rises to 2.8% for *RF-Egg-S* and 2.3% for *RF-Egg-P* with 16 targets. It can be observed that the performance decreases in both metrics as the number of multi-targets grows due to the introduction of more complex multipath environments and signal interference. Additionally, the slightly inferior performance of *RF-Egg-S* compared to *RF-Egg-P* is primarily attributed to the longer distance and no egg fixation settings.

Result of Task 2. For Task 2, *RF-Egg* has achieved an average Acc. of 91.2% and 92.4%, along with an average MAD of 0.7 and 0.6, for *RF-Egg-S* and *RF-Egg-P*, respectively. Specifically, the Acc. and MAD curves for *RF-Egg-S* and *RF-Egg-P* follow an increasing and decreasing pattern as the multi-target number increases from 1 to 16. The Acc. is 84.4% for

[4]Ethical consideration: Animal ethical approval has been granted by the corresponding organization. All the hatched chickens were properly handled.

Table 2: Summary of candidate eggs.

Physical Property	Density			Shape Index (SI)			Incubation Condition (Groundtruth)		
	Mass (g)	Length (mm)	Width (mm)	<0.72	0.72–0.76	>0.76	Non-Fertilized	Fertilized	Early-Mortal
Detail	44.3–63.4 (52.9)	49.1–54.7 (52.6)	37.6–42.1 (39.2)	53	107	29	18	137	34

SI is a geometric parameter defined as the ratio of width to length [1], generally sharp eggs (<0.72), standard eggs (0.72–0.76) and round eggs (>0.76). Mean values are presented in parentheses.

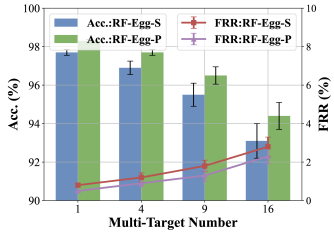

Fig. 13: Result of Task 1.

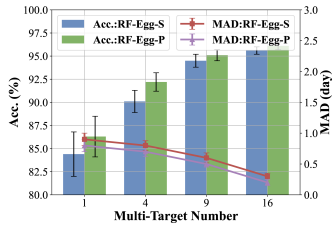

Fig. 14: Result of Task 2.

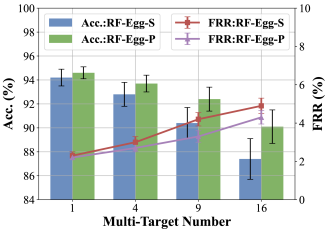

Fig. 15: Result of Task 3.

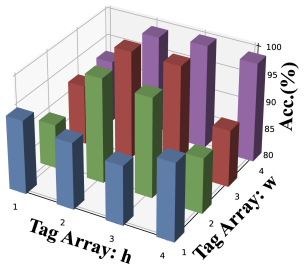

Fig. 16: Impact of tag location.

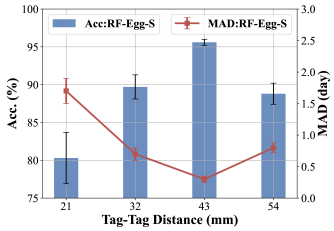

Fig. 17: Impact of tag-tag distance.

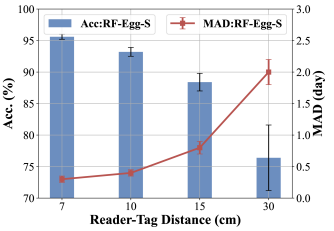

Fig. 18: Impact of reader-tag distance.

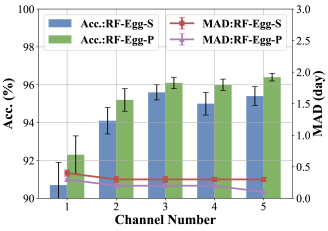

Fig. 19: Impact of data source.

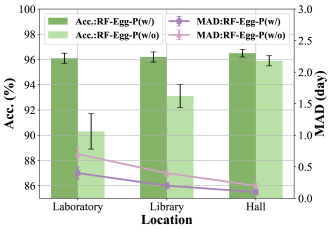

Fig. 20: Impact of multipath.

RF-Egg-S and 86.3% for *RF-Egg-P* with one single sensing target, but it grows to 95.6% and 96.1% when sensing 16 targets. The main reason for this trend is that we utilize GM as the feature map for Task 2, where multiple eggs contribute to the result, providing reliability and robustness for *RF-Egg*. Similarly, the MAD for *RF-Egg-S* and *RF-Egg-P* with one single target is 0.9 and 0.8, respectively, but decreases to 0.3 for *RF-Egg-S* and 0.2 for *RF-Egg-P* with 16 targets.

Result of Task 3. Similarly for Task 3, *RF-Egg* has achieved an average Acc. of 91.2% and 92.7%, along with an average FRR of 3.6% and 3.1%, for *RF-Egg-S* and *RF-Egg-P*, respectively. When sensing one target, *RF-Egg-S* and *RF-Egg-P* achieve an Acc. of 94.2% and 94.6%, respectively. However, when sensing 16 targets, there is a decline in performance, dropping to 87.4% for *RF-Egg-S* and 90.1% for *RF-Egg-P*. The FRR for *RF-Egg-S* and *RF-Egg-P* is 2.3% and 2.2%, while it escalates to 4.9% and 4.3% when sensing 16 targets.

7.3 Micro-benchmarking

We now evaluate the performance of *RF-Egg* with respect to different tag locations, tag-tag distances, reader-tag distances, data sources, and multipath levels.

7.3.1 Impact of Tag Location. Fig. 16 illustrates the performance of *RF-Egg-P* in Task 1 across 16 different tag locations in the tag array Γ with the size of $h \times w$ ($h = w = 4$). It is observed that the Acc. fluctuates depending on the tag positions, albeit the variations are not drastically large. Tags situated at the center of the tag array slightly exhibit superior performance compared to those at the edges. Quantitatively, the centrally four positioned tags attain an average Acc. of 98.9%, excelling the 92.9% achieved by the edge-located tags. This discrepancy can be attributed to the fact that the edge tags tend to yield sparse and unstable RFID response sequences.

7.3.2 Impact of Tag-Tag Distance. Fig. 17 illustrates the performance of *RF-Egg-S* in Task 2 across different tag-tag distances with respect to four distances of 21 mm, 32 mm, 43 mm (default one), and 54 mm. We can observe that the performance of *RF-Egg-S* is significantly influenced by the distance between tags. At the shortest distance of 21 mm, the Acc. and MAD are 80.3% and 1.7, respectively. However, when the distance is extended to 43 mm, there is a noticeable improvement in performance, with the Acc. surging to 95.6% and the MAD reducing to 0.3. This can be ascribed that the proximity of the eggs influences the weak coupling effect

between the tag and its corresponding targets, resulting in suboptimal performance. However, it is noted that overly large distances present their own set of challenges, primarily due to the limited beam range of the directional antenna and communication complications with the edge label. This is manifested by a decrease in Acc. to 88.8% and MAD to 0.8 at a distance of 54 mm.

7.3.3 Impact of Reader-Tag Distance. Fig. 18 showcases the performance of *RF-Egg-S* in Task 2 across different reader('s antenna)-tag distances, specifically at four distances 7 cm (default one), 10 cm, 15 cm, and 30 cm. We can observe that the Acc. curves and MAD curves of *RF-Egg-S* show a decreasing and increasing trend as reader-tag distances increase, respectively. At a distance of 7 cm, *RF-Egg-S* achieves an Acc. of 95.6% and a MAD of 0.3. However, at a distance of 30 cm, the performance decreases, with the Acc. dropping to 76.4% and the MAD rising to 2.0. This performance degradation is primarily due to the RFID backscatter signal becoming weak at larger distances, which can even lead to communication breakdowns. However, this issue can be mitigated through hardware substitution, enabling *RF-Egg* to operate effectively at more desirable distances.

7.3.4 Impact of Data Source. Fig. 19 showcases the performance of *RF-Egg* in Task 2 under varying numbers of channels in the feature map, spanning from 1 to 5. The Acc. and MAD curves of *RF-Egg* display an ascending and descending trend as the number of channels increases, but start to level off when the channel count reaches 3. This can be attributed to the ideally linearly-varying phase data across multiple RFID hopping channels as elaborated in §5.1. Specifically, increasing the number of channels can enhance the stability of the feature map, but it does not contribute additional insightful information.

7.3.5 Impact of Multipath. Fig. 20 illustrates the performance of *RF-Egg-P* in three distinct environments: a laboratory, a library, and a hall, which represents a decreasing level of multipath interference. We can observe *RF-Egg-P* with the proposed multipath combating algorithm achieves a stable average Acc. of 96.3% and MAD of 0.2. While *RF-Egg-P* without the algorithm experiences a slight improvement in performance in environments with diminished multipath interference, from 90.3% to 95.9% in Acc. and from 0.7 to 0.2 in MAD. This implies that *RF-Egg-P* is sensitive to the external environment and can benefit from multipath combating.

7.4 Field Study

Experimental setup in field study. As shown in Fig. 21, we conducted a field study of *RF-Egg* at a local egg hatchery under the guidance of professionals over three days. Specifically, we used *RF-Egg-P* configuration to measure 80 eggs per

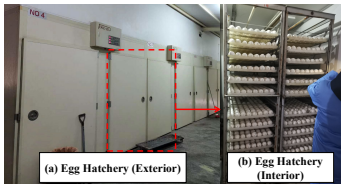

Fig. 21: Field study.

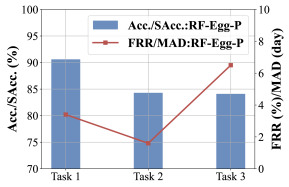

Fig. 22: Result of field study.

day (a total of 240 ones) in an empty room under single-target settings. We measured each egg three times a day, taking two samples each time. These samples were processed as feature maps for the corresponding tasks, and then fed into our trained network for testing. It is noted that, for Task 2, we use Soft Accuracy (SAcc.) as the performance metric, which is defined as the ratio of the samples that are classified within two classes adjacent to their true labels over the total number of samples.

Results of field study. Fig. 22 showcases the results of our field study. Specifically, for Task 1, we achieved an Acc. of 90.6% and FRR of 3.4%. For Task 2, we obtained an SAcc. of 84.3% and MAD of 1.6. For Task 3, these metrics were 84.1% and 6.5%, respectively. These results affirm the effectiveness of *RF-Egg* in the modern poultry industry.

8 LIMITATIONS AND FUTURE WORKS

We briefly delve into a few of concerns below.

Robustness. Robustness poses a significant challenge in wireless sensing, as the data measurement can be influenced by the experimental setup (e.g., stationary/portable settings and collection time), target properties (e.g., size/weight and flip), and environmental conditions (e.g., temperature/humidity and multipath). Thus, the performance of *RF-Egg* may be constrained by the accuracy of the data measurement, given that the phase readings of RF signals are fine-grained but also highly sensitive. In industrial deployments, enhanced performance can be likely achieved with more precise settings.

Distance challenge. Both the tag-tag and reader-tag distances have a substantial impact on sensing accuracy, given the fine-grained nature of egg incubation sensing. Interference is more likely to occur at close tag-to-tag distances, which can potentially degrade performance. Similarly, at longer reader-to-tag distances, communication breakdowns are more likely, which could also negatively affect the system's efficacy and limit its practical usage. Though substituting the hardware may address these issues, we choose to explore other potential solutions in our future works.

Applications in poultry industry. *RF-Egg*, as a proof of concept, delves into the potential of RF signals in the field of chicken egg incubation sensing, showcasing its potential for

various aspects of the poultry industry. For example, when extrapolating this to the eggs of other species, the designed three tasks and their respective solutions still remain applicable. This suggests the potential versatility and scalability of *RF-Egg*, making it a valuable tool in the advancement of the modern poultry industry. In the meantime, the real-time capability still requires to be explored.

9 RELATED WORKS

In this section, we briefly review several aspects of related work.

Incubation-related sensing. Current incubation-related sensing works are primarily designed for egg fertility detection, involving vision-based and sensor-based ones. Traditional vision-based methods utilize embryo candling [14, 39], hyper-spectral imaging [28], and thermal imaging [25] to acquire high-resolution image data for classification tasks. Saifullah et al. [39] extracted Gray-Level Co-occurrence Matrix (GLCM) based on the candling images for Support Vector Machine (SVM) to perform egg fertility detection on day 5 of incubation. Similarly, Liu et al. [28] first segmented the Region Of Interest (ROI) of hyper-spectral and then extracted MS (mean spectra of ROI) and MG (mean spectra of the Gabor-filtered ROI) for further classification. While sensor-based methods focus on the variation of inherent properties during incubation with respect oxygen flux [37], resonance analysis [6], dielectric properties [15], spectral analysis [10]. Wang et al. [37] concluded there is a significant difference in gas exchange rates between fertilized and non-fertilized eggs. Coucke et al. [6] measured the frequency response of a chicken egg excited with an impact excitation to detect egg fertility on day 5 of incubation. Differently, *RF-Egg* is the first RF-based work achieving multi-target and multi-task egg incubation sensing, possessing the characteristics of non-intrusiveness, high-responsiveness, and well-usability.

RFID sensing. The sensing potential of RFID has garnered significant attention for a long time, particularly in the areas of fine-grained tracking [22, 23], localization [9, 45], material identification [47, 50], and gesture sensing [52]. OmniTrack [22] achieves tracking accuracy by quantifying the respective impact of the read-tag distance and the tag's orientation at the centimeter-level. Tagtag [50] and RF-EATS [16] leverage the weak coupling effects that the tag antenna impedance changes when interacting with the target to achieve different material identification. While TagScan [47] captures different amounts of RSS and phase variation when RF signals penetrate different materials. EU-IGR [52] extracts the environment and user invariant features from RSS and phase readings through adversarial learning for gesture recognition. RF-DNA [35] achieves physical-layer identification by proposing a novel hardware fingerprint representing the tag's intrinsic response at some frequency. Additionally, RFID technology has also been applied for soil moisture sensing [46], temperature sensing [36], infusion drip rate monitoring [26], user authentication [27], etc. Compared with these works, *RF-Egg* fills the gap of egg incubation sensing.

Other wireless signal sensing. Apart from RFID technology, other wireless signals with different frequency bands have been explored for their sensing capabilities, such as Wi-Fi [13, 21, 41, 48], radar [18, 20, 38], LoRa [51, 55], acoustic [5, 11, 29], ZigBee [54], etc. For example, DroneScale [31] achieves drone load sensing by leveraging the RF signals transmitted by commercial drones. mmRipple [7] empowers the communication capability between mmWave radar and vibrating smartphone. Mobi^{2}Sense [56] achieves UWB sensing capability under device motions. In addition, AppListener [32] leverages the RF energy in network traffic to recognize mobile app activities.

10 CONCLUSION

This paper presents the design, implementation, and evaluation of *RF-Egg*, to achieve fine-grained multi-target and multi-task egg incubation sensing, which possesses the characteristics of non-intrusiveness, high-responsiveness, and well-usability. *RF-Egg* utilizes an RFID tag array where each tag corresponds to each egg, and leverages the low-level phase readings to achieve egg incubation sensing with respect to fertility, incubation status, and early mortality. Specifically, we propose a multipath combating algorithm to extract the target-induced signal component and address non-uniformity issues across multiple tags. Subsequently, we design an MTT network to consider task-specific input, network architecture, and task imbalance problems. The experiment results show that *RF-Egg* can achieve an accuracy of 94.4%, 96.1%, and 90.1% for the three tasks when supporting 16 targets simultaneously. Additionally, our field study suggests that *RF-Egg* holds significant potential for the modern poultry industry.

ACKNOWLEDGMENTS

We sincerely thank the anonymous shepherd and reviewers for their constructive comments. The work was supported by the Research Grants Council of the Hong Kong Special Administrative Region, China (Project No. CityU 21201420 and CityU 11201422), and CityU MFPRC grant 9680333, CityU SIRG grant 7020057, CityU SRG-Fd 7005984. Any opinions, findings, and conclusions in this paper are those of the authors and not necessarily of the supported organizations.

REFERENCES

[1] Ebubekir Altuntaş and Ahmet Şekeroğlu. 2008. Effect of egg shape index on mechanical properties of chicken eggs. *Elsevier J. Food Eng.* (2008).

[2] V Ballenegger and J-P Hansen. 2005. Dielectric permittivity profiles of confined polar fluids. *AIP J. Chem. Phys.* (2005).

[3] Roberto Battiti. 1992. First-and second-order methods for learning: between steepest descent and Newton's method. *MIT Press Neural Comput.* (1992).

[4] Rahul Bhattacharyya, Christian Floerkemeier, and Sanjay Sarma. 2010. Low-cost, ubiquitous RFID-tag-antenna-based sensing. *Proceedings of IEEE* (2010).

[5] Yongliang Chen, Tao Ni, Weitao Xu, and Tao Gu. 2022. SwipePass: Acoustic-based Second-factor User Authentication for Smartphones. *ACM IMWUT* (2022).

[6] Peter M Coucke, Gwendolien M Room, Eddy M Decuypere, and Josse G De Baerdemaeker. 1997. Monitoring embryo development in chicken eggs using acoustic resonance analysis. *Wiley Biotechnology progress* (1997).

[7] Kaiyan Cui, Qiang Yang, Yuanqing Zheng, and Jinsong Han. 2023. mmRipple: Communicating with mmWave Radars through Smartphone Vibration. In *Proceedings of ACM/IEEE IPSN.*

[8] Daniel Dobkin. 2012. *The rf in RFID: uhf RFID in practice.*

[9] Laura Dodds, Isaac Perper, Aline Eid, and Fadel Adib. 2023. A Handheld Fine-Grained RFID Localization System with Complex-Controlled Polarization. *Proceedings of ACM MobiCom* (2023).

[10] Jun Dong, Xiaoguang Dong, Yanlei Li, Beibei Zhang, Lingjuan Zhao, Kuanglin Chao, and Xiuying Tang. 2020. Prediction of infertile chicken eggs before hatching by the Naïve-Bayes method combined with visible near infrared transmission spectroscopy. *Taylor & Francis Spectroscopy Letters* (2020).

[11] Di Duan, Yongliang Chen, Weitao Xu, and Tianxing Li. 2024. EarSE: Bringing Robust Speech Enhancement to COTS Headphones. *ACM IMWUT* (2024).

[12] Walter Gander, Gene H Golub, and Rolf Strebel. 1994. Least-squares fitting of circles and ellipses. *Springer BIT Numer. Math.* (1994).

[13] Chuhan Gao, Yilong Li, and Xinyu Zhang. 2019. Livetag: Sensing human-object interaction through passive chipless wi-fi tags. *Proceedings of ACM NSDI* (2019).

[14] Lei Geng, Yunyun Xu, Zhitao Xiao, and Jun Tong. 2020. DPSA: dense pixelwise spatial attention network for hatching egg fertility detection. *SPIE Journal of Electronic Imaging* (2020).

[15] Mahdi Ghaderi, Ahmad Banakar, and Ali Akbar Masoudi. 2018. Using dielectric properties and intelligent methods in separating of hatching eggs during incubation. *Elsevier Measurement* (2018).

[16] Unsoo Ha, Junshan Leng, Alaa Khaddaj, and Fadel Adib. 2020. Food and liquid sensing in practical environments using rfids. In *Proceedings of NSDI.*

[17] Robert Hadek. 1965. The structure of the mammalian egg. *Elsevier Int. Rev. Cytol.* (1965).

[18] Mingda Han, Huanqi Yang, Tao Ni, Di Duan, Mengzhe Ruan, Yongliang Chen, Jia Zhang, and Weitao Xu. 2023. mmSign: mmWave-based Few-Shot Online Handwritten Signature Verification. *ACM TOSN* (2023).

[19] Kaiming He, Xiangyu Zhang, Shaoqing Ren, and Jian Sun. 2016. Deep residual learning for image recognition. In *Proceedings of IEEE CVPR.*

[20] Chen-Yu Hsu, Rumen Hristov, Guang-He Lee, Mingmin Zhao, and Dina Katabi. 2019. Enabling identification and behavioral sensing in homes using radio reflections. In *Proceedings of ACM CHI.*

[21] Sijie Ji, Yaxiong Xie, and Mo Li. 2022. SiFall: Practical Online Fall Detection with RF Sensing. In *Proceedings of ACM SenSys.*

[22] Chengkun Jiang, Yuan He, Xiaolong Zheng, and Yunhao Liu. 2018. Orientation-aware RFID tracking with centimeter-level accuracy. In *Proceedings of ACM/IEEE IPSN.*

[23] Haojian Jin, Zhijian Yang, Swarun Kumar, and Jason I Hong. 2018. Towards wearable everyday body-frame tracking using passive RFIDs. *ACM IMWUT* (2018).

[24] Qiuhong Ke, Mohammed Bennamoun, Senjian An, Ferdous Sohel, and Farid Boussaid. 2017. A new representation of skeleton sequences for 3d action recognition. In *Proceedings of IEEE CVPR.*

[25] Chern-Sheng Lin, Po Ting Yeh, Der-Chin Chen, Yih-Chih Chiou, and Chi-Hung Lee. 2013. The identification and filtering of fertilized eggs with a thermal imaging system. *Elsevier Computers and Electronics in Agriculture* (2013).

[26] Yuancan Lin, Lei Xie, Chuyu Wang, Yanling Bu, and Sanglu Lu. 2021. Dropmonitor: Millimeter-level sensing for RFID-based infusion drip rate monitoring. *ACM IMWUT* (2021).

[27] Jianwei Liu, Kaiyan Cui, Xiang Zou, Jinsong Han, Feng Lin, and Kui Ren. 2022. Reliable Multi-Factor User Authentication With One Single Finger Swipe. *IEEE/ACM TON* (2022).

[28] L Liu and MO Ngadi. 2013. Detecting fertility and early embryo development of chicken eggs using near-infrared hyperspectral imaging. *Springer Food and Bioprocess Technology* (2013).

[29] Tiantian Liu, Ming Gao, Feng Lin, Chao Wang, Zhongjie Ba, Jinsong Han, Wenyao Xu, and Kui Ren. 2021. Wavoice: A noise-resistant multi-modal speech recognition system fusing mmwave and audio signals. In *Proceedings of ACM SenSys.*

[30] Jianwen Luo, Kui Ying, and Jing Bai. 2005. Savitzky–Golay smoothing and differentiation filter for even number data. *Elsevier Signal Processing* (2005).

[31] Phuc Nguyen, Vimal Kakaraparthi, Nam Bui, Nikshep Umamahesh, Nhat Pham, Hoang Truong, Yeswanth Guddeti, Dinesh Bharadia, Richard Han, Eric Frew, et al. 2020. DroneScale: drone load estimation via remote passive RF sensing. In *Proceedings of SenSys.*

[32] Tao Ni, Guohao Lan, Jia Wang, Qingchuan Zhao, and Weitao Xu. 2023. Eavesdropping Mobile App Activity via {Radio-Frequency} Energy Harvesting. In *Proceedings of USENIX Security.*

[33] Pavel V Nikitin, KVS Rao, and Steve Lazar. 2007. An overview of near field UHF RFID. In *IEEE RFID.*

[34] United States Department of Agriculture(USDA)/National Agricultural Statistics Service(NASS). 2023. USDA/NASS Poultry Production and Value 2022 Summary. https://www.uspoultry.org/economic-data/.

[35] Qingrui Pan, Zhenlin An, Xueyuan Yang, Xiaopeng Zhao, and Lei Yang. 2022. RF-DNA: large-scale physical-layer identifications of RFIDs via dual natural attributes. In *Proceedings of ACM MobiCom.*

[36] Swadhin Pradhan and Lili Qiu. 2020. Rtsense: passive rfid based temperature sensing. In *Proceedings of ACM MobiSys.*

[37] Wang Qiaohua, Fu Dandan, Ma Meihu, and Zhang Tao. 2017. Differentiating between fertilized and unfertilized eggs prior to incubation based on oxygen flux measurement. *CSAE International Journal of Agricultural and Biological Engineering* (2017).

[38] Tauhidur Rahman, Alexander T Adams, Ruth Vinisha Ravichandran, Mi Zhang, Shwetak N Patel, Julie A Kientz, and Tanzeem Choudhury. 2015. Dopplesleep: A contactless unobtrusive sleep sensing system using short-range doppler radar. In *Proceedings of ACM UbiComp.*

[39] Shofan Saifullah and Rafał Drężewski. 2022. Non-Destructive Egg Fertility Detection in Incubation Using SVM Classifier Based on GLCM Parameters. *Elsevier Procedia Computer Science* (2022).

[40] Florian Schroff, Dmitry Kalenichenko, and James Philbin. 2015. Facenet: A unified embedding for face recognition and clustering. In *Proceedings of IEEE CVPR.*

[41] Yuanchao Shu, Cheng Bo, Guobin Shen, Chunshui Zhao, Liqun Li, and Feng Zhao. 2015. Magicol: Indoor localization using pervasive

magnetic field and opportunistic WiFi sensing. *IEEE JSAC* (2015).
[42] Pirapat Tangsuknirundorn and Pitikhate Sooraksa. 2019. Design of a cyber-physical system using stem: chicken egg incubator. In *IEEE ICEAST*.
[43] SG Tullett. 1990. Science and the art of incubation. *Elsevier Poultry Science* (1990).
[44] Simon Vandenhende, Stamatios Georgoulis, Wouter Van Gansbeke, Marc Proesmans, Dengxin Dai, and Luc Van Gool. 2021. Multi-task learning for dense prediction tasks: A survey. *IEEE TPAMI* (2021).
[45] Ge Wang, Chen Qian, Longfei Shangguan, Han Ding, Jinsong Han, Nan Yang, Wei Xi, and Jizhong Zhao. 2017. HMRL: Relative localization of RFID tags with static devices. In *Proceedings of IEEE SECON)*.
[46] Ju Wang, Liqiong Chang, Shourya Aggarwal, Omid Abari, and Srinivasan Keshav. 2020. Soil moisture sensing with commodity RFID systems. In *Proceedings of ACM MobiSys*.
[47] Ju Wang, Jie Xiong, Xiaojiang Chen, Hongbo Jiang, Rajesh Krishna Balan, and Dingyi Fang. 2017. TagScan: Simultaneous target imaging and material identification with commodity RFID devices. In *Proceedings of ACM MobiCom*.
[48] Chenhao Wu, Xuan Huang, Jun Huang, and Guoliang Xing. 2023. Enabling Ubiquitous WiFi Sensing with Beamforming Reports. In *Proceedings of the ACM SIGCOMM*.
[49] Chenshu Wu, Feng Zhang, Beibei Wang, and KJ Ray Liu. 2020. msense: Towards mobile material sensing with a single millimeter-wave radio. *ACM IMWUT* (2020).
[50] Binbin Xie, Jie Xiong, Xiaojiang Chen, Eugene Chai, Liyao Li, Zhanyong Tang, and Dingyi Fang. 2019. Tagtag: material sensing with commodity RFID. In *Proceedings of ACM SenSys*.
[51] Huanqi Yang, Mingda Han, Mingda Jia, Zehua Sun, Pengfei Hu, Yu Zhang, Tao Gu, and Weitao Xu. 2023. XGait: Cross-Modal Translation via Deep Generative Sensing for RF-based Gait Recognition. In *Proceedings of ACM SenSys*.
[52] Yinggang Yu, Dong Wang, Run Zhao, and Qian Zhang. 2019. RFID based real-time recognition of ongoing gesture with adversarial learning. In *Proceedings of ACM SenSys*.
[53] Zhiyuan Yu, Zhuohang Li, Yuanhaur Chang, Skylar Fong, Jian Liu, and Ning Zhang. 2022. HeatDeCam: Detecting Hidden Spy Cameras via Thermal Emissions. In *Proceedings of ACM CCS*.
[54] R Ivan Zelaya, William Sussman, Jeremy Gummeson, Kyle Jamieson, and Wenjun Hu. 2021. LAVA: fine-grained 3D indoor wireless coverage for small IoT devices. In *Proceedings of ACM SIGCOMM*.
[55] Fusang Zhang, Zhaoxin Chang, Jie Xiong, Rong Zheng, Junqi Ma, Kai Niu, Beihong Jin, and Daqing Zhang. 2021. Unlocking the beamforming potential of lora for long-range multi-target respiration sensing. *ACM IMWUT* (2021).
[56] Fusang Zhang, Jie Xiong, Zhaoxin Chang, Junqi Ma, and Daqing Zhang. 2022. Mobi2Sense: empowering wireless sensing with mobility. In *Proceedings of ACM MobiCom*.
[57] Yu Zhang and Qiang Yang. 2021. A survey on multi-task learning. *IEEE TKDE* (2021).